The Journal of Chemical Physics

Effect of ammonium fluoride doping on the ice III to ice IX phase transition

Cite as: J. Chem. Phys. **154**, 114502 (2021); https://doi.org/10.1063/5.0032485
Submitted: 08 October 2020 • Accepted: 15 February 2021 • Published Online: 15 March 2021

Zainab Sharif, Jacob J. Shephard, Ben Slater, et al.

The Journal of Chemical Physics ARTICLE scitation.org/journal/jcp

Effect of ammonium fluoride doping on the ice III to ice IX phase transition

Cite as: J. Chem. Phys. 154, 114502 (2021); doi: 10.1063/5.0032485
Submitted: 8 October 2020 • Accepted: 15 February 2021 •
Published Online: 15 March 2021

Zainab Sharif,[1] Jacob J. Shephard,[1] Ben Slater,[1] Craig L. Bull,[2] Martin Hart,[1] and Christoph G. Salzmann[1,a)]

AFFILIATIONS

[1] Department of Chemistry, University College London, 20 Gordon Street, London WC1H 0AJ, United Kingdom
[2] ISIS Pulsed Neutron and Muon Source, Rutherford Appleton Laboratory, Harwell Oxford, Didcot OX11 0QX, United Kingdom

[a)] Author to whom correspondence should be addressed: c.salzmann@ucl.ac.uk

ABSTRACT

Ice III is a hydrogen-disordered phase of ice that is stable between about 0.2 and 0.35 GPa. Upon cooling, it transforms to its hydrogen-ordered counterpart ice IX within the stability region of ice II. Here, the effect of ammonium fluoride doping on this phase transition is investigated, which is followed for the first time with *in situ* neutron diffraction. The *a* and *c* lattice constants are found to expand and contract, respectively, upon hydrogen ordering, yielding an overall negative volume change. Interestingly, the anisotropy in the lattice constants persists when ice IX is fully formed, and negative thermal expansion is observed. Analogous to the isostructural keatite and β-spodumenes, the negative thermal expansion can be explained through the buildup of torsional strain within the *a*–*b* plane as the helical "springs" within the structure expand upon heating. The reversibility of the phase transition was demonstrated upon heating. As seen in diffraction and Raman spectroscopy, the ammonium fluoride doping induces additional residual hydrogen disorder in ice IX and is suggested to be a chemical way for the "excitation" of the configurational ice-rules manifold. Compared to ice VIII, the dopant-induced hydrogen disorder in ice IX is smaller, which suggests a higher density of accessible configurational states close to the ground state in ice IX. This study highlights the importance of dopants for exploring the water's phase diagram and underpins the highly complex solid-state chemistry of ice.

INTRODUCTION

Ice III occupies the smallest region of thermodynamic stability in the phase diagram of H_2O.[1,2] As shown in Fig. 1(a), it is stable between approximately 0.2 and 0.35 GPa, and over a temperature range of ~10 K sharing triple points with the "ordinary" ice I*h*, ice II, ice V, and liquid water.[3–5] Since ice III forms at quite moderate pressures, it may be part of the ice shells of several of the icy moons in the solar system.[6–8] Its hydrogen-bonded network of water molecules is isostructural with the keatite silica polymorph and described by the tetragonal $P4_12_12$ space group.[9–13] This makes ice III a chiral phase of ice,[1] together with the recently discovered ice XVII.[14] The unit cells of ice III using the $P4_12_12$ space group and its enantiomorphic counterpart $P4_32_12$ are shown in Fig. 1(b). The structures contain two crystallographically distinct oxygen sites and three different types of hydrogen bonds. A defining structural feature is four-fold spirals along the crystallographic *c* axis, which, depending on the space group, display a different handedness. The spirals contain one type of hydrogen bond, whereas the other two arise from water molecule hydrogen bonding to four neighboring spirals.[9–12]

Originally, the hydrogen-bonded water molecules in ice III were believed to be fully orientationally disordered.[15,16] In diffraction, such a fully hydrogen-disordered structure can be described with half-occupied hydrogen sites reflecting the average structure. However, *in situ* neutron diffraction of ice III in its region stability has shown that the fractional occupancies of the six crystallographically distinct deuterium sites deviate from $\frac{1}{2}$.[17–19] Considering the ice rules, the six occupancies can be described with two order parameters α and β ranging from 0 to 1 and, hence, can define the extent of hydrogen (dis)order of the hydrogen bonds between and within the four-fold spirals, respectively.[12] At 250 K and 0.3 GPa, α and β were found to take values of 0.36 and 0.53.[19] The small deviations from $\frac{1}{2}$ mean that ice III is classified as a partially ordered hydrogen-disordered phase of ice.

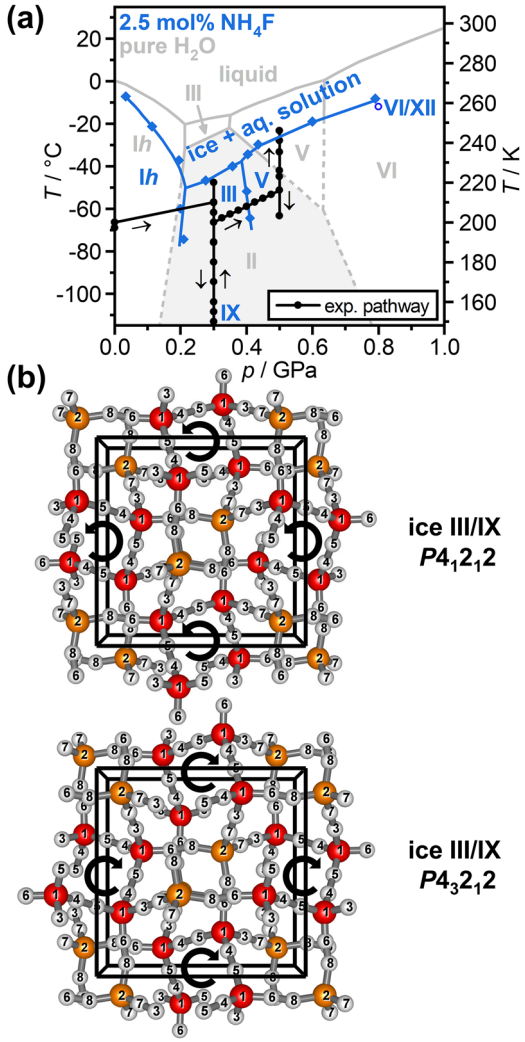

FIG. 1. (a) Phase diagram of pure ice (gray) and ice with 2.5 mol. % NH_4F (blue).[20] The experimental pathway using 2.5 mol. % ND_4F in this study is indicated by full black circles. (b) Unit cell of ice III/IX using the $P4_12_12$ space group (top) as well as the corresponding enantiomorphic space group $P4_32_12$ (bottom). The crystallographically distinct oxygen sites are shown as red and orange spheres, and the hydrogen sites as smaller white spheres. The labeling of the atoms is as defined in Ref. 12. The circular arrows indicate the handedness of the four-fold screw axes.

Upon cooling under pressure, ice III transforms to its antiferroelectric hydrogen-ordered counterpart ice IX between 208 and 165 K.[21] In Kurt Vonnegut's novel *Cat's Cradle*, "ice-nine" is a fictional deadly form of ice that is stable under ambient conditions.[21,22] In stark contrast to this, the real ice IX is always metastable with respect to ice II at temperatures below the region of stability of ice III.[23] Due to its metastability, ice IX is often found in sequences of phase transitions at low temperatures following Ostwald's rule of stages up to ~0.7 GPa.[24,25] Using single-crystal neutron diffraction, it was shown that D_2O ice IX contains a small amount of residual hydrogen disorder (α = 0.034 and β = 0.051).[12,17] The ice III to ice IX phase transition is the only hydrogen-ordering phase transition in ice observed so far, where the space group symmetry does not change.[9–12,17,26–29] Using density functional theory (DFT) calculations, the experimental structure of ice IX was shown to display the lowest energy out of the four possible ordered arrangements in $P4_12_12$.[30]

The phase transition from ice III to ice IX upon cooling under pressure was previously followed with dielectric spectroscopy,[21] calorimetry,[31] and Raman spectroscopy.[32] It was found that cooling rates greater than 1–2 K min^{-1} are needed in order to suppress the transformation to the stable ice II.[32,33] Upon heating, ice IX transforms to the stable ice II typically between 190 and 210 K.[3,21,31,32] So far, the phase transition has not been followed by diffraction techniques.

Recently, we have shown that the fully hydrogen-ordered ice II can be selectively destabilized using small amounts of ammonium fluoride (NH_4F) doping so that ice III becomes the stable phase at 0.3 GPa.[20] The mechanism for this is that NH_4F acts as a hydrogen disordering agent, which has also recently been demonstrated for the ice VII to ice VIII phase transition.[34] Since ice III is already hydrogen-disordered, its free energy is not significantly affected by the NH_4F dopant.

Ice and NH_4F have generally been found to mix very well. At ambient pressure, for example, ice I*h* forms a solid solution with NH_4F up to ~8 mol. %, which is followed by the formation of monohydrate at higher NH_4F concentrations.[35–37] At the other end of the composition range and on the basis of the hygroscopic nature of NH_4F, it can be assumed that solid solutions of H_2O in NH_4F-I exist. NH_4F-I is isostructural with ice I*h*, but stacking-disordered versions of NH_4F-I have been shown to exist.[38] The high solubility of NH_4F in ice has been explained by the similar length of the O–H···O and N–H···F hydrogen bonds, which differ by less than 2%.[39] The lengths of the mixed O–H···F and N–H···O hydrogen bonds in solid solutions can be expected to be even more similar compared to the O–H···O hydrogen bonds. In addition to ice I*h*, NH_4F has been shown to be soluble in clathrate hydrates.[40,41] The solubility of NH_4F in ice III was demonstrated on the basis of small changes in the lattice constants as a function of NH_4F concentration.[20] Furthermore, it was shown computationally that there is no energetic gain for bringing the NH_4^+ and F^- ions into close contact within an ice III matrix, which would represent the first step for phase separation.[20] Overall, the solubility of NH_4F in ice materials is highly remarkable since most other ionic species such as NaCl display very low solubilities in ice.[23]

Here, we investigate the effect of 2.5 mol. % ammonium fluoride doping on the ice III to ice IX phase transition upon isobaric cooling at 0.3 GPa using *in situ* neutron diffraction, and we test the reversibility of the phase transition upon isobaric heating. The hydrogen-disordering effect of the dopant on ice IX is quantified and compared with the effects found for ice VIII. Using density functional theory, the differences in the lattice constants between ice III and ice IX are predicted for the pure ices and compared with the experimental ones obtained from the doped sample. The hydrogen-disordering effect of ammonium fluoride on ice IX is also followed with Raman spectroscopy as a function of the ammonium fluoride concentration. Finally, we investigate the phase transitions of ammonium fluoride doped ices as the pressure is increased to 0.5 GPa.

EXPERIMENTAL AND COMPUTATIONAL METHODS

Deuterated ammonium fluoride (ND_4F) was obtained by dissolving NH_4F (99.99% trace metal basis) in an excess of deuterated water (99.9% D) followed by the complete evaporation of the liquid by boiling under a constant flow of dry nitrogen gas. To ensure complete deuteration, the dissolution in D_2O followed by evaporation was repeated twice. The resulting dry ND_4F powder was stored in a desiccator and used to prepare a 2.5 mol. % solution in D_2O. Complete deuteration was confirmed from the absence of N–H stretching modes in Raman spectroscopy. All ND_4F solutions were prepared and handled in polyethylene containers.

A few milliliters of the 2.5 mol. % solution were frozen in a porcelain pestle and mortar precooled with liquid nitrogen. After grinding for a few minutes, the fine powder was transferred into a cylindrical TiZr cell with a Bridgman seal at the bottom, which was attached to a gas-intensifier unit while keeping the pressure cell cold with external dry ice. Argon gas was used as a pressure medium. To create a seal, the pressure was quickly increased to 1500 bars and then released again. For temperature measurements, a thermocouple was attached to the TiZr cell with a copper ring. The gas cell was then mounted onto a cryostat stick and lowered into a helium cryostat precooled to 200 K on the PEARL beamline at ISIS.[42] The temperature/pressure pathways of the experiment are shown in Fig. 1(a). For ices III/IX, two long runs were recorded at 210 and 150 K for 1500 μA h of proton current (~10 h), while shorter runs of 150 μA h (~1 h) were recorded at the other temperatures. All neutron diffraction patterns were collected at 90° scattering angle and analyzed using the GSAS software.[43] The ice IX structure from Ref. 12 was generally found to be the best start structure for the refinements.

For Raman spectroscopy, H_2O ice III/IX samples with 0, 2.5, and 5.0 mol. % NH_4F were prepared by isobaric heating of ice I*h* at 0.3 GPa using a piston cylinder setup as described in Ref. 20. To be able to record decoupled O–D stretching modes, each sample contained 5 mol. % deuterium. Once the ice III had formed, the samples were quenched with liquid nitrogen while maintaining the pressure at 0.3 GPa. Upon reaching liquid nitrogen temperature, the samples were decompressed, recovered from the pressure die under liquid nitrogen, and transferred into a Microstat^N cryostat from Oxford Instruments precooled to 80 K. The Raman spectra of the samples were recorded at 80 K using a Renishaw Ramascope spectrometer equipped with a 632.8 nm He–Ne laser in static mode and co-adding four spectra.

In addition to the *in situ* neutron diffraction experiments at 0.5 GPa with a 2.5 mol. % ND_4F-doped sample, pure ice I*h* and doped H_2O samples with 0.05, 0.10, 0.25, 0.50, 1.00, and 2.50 mol. % NH_4F were heated isobarically at 0.5 GPa and ~3 K min^{-1} in a hardened-steel pressure die from liquid nitrogen temperature to the melting point while recording the piston displacements required to keep the pressure constant. The ice samples were encased in indium cups, and the melting point was detected from water leaking from the pressure setup, which was often accompanied by a "creaking" sound. The phase identities of the samples at various temperatures and NH_4F concentrations were confirmed with x-ray diffraction.[44]

Density functional theory calculations were performed with the quickstep module of the CP2K code[45] using the PBE (Perdew-Burke-Ernzerhof) functional, and dispersion corrections were implemented through the Grimme D3 scheme.[46] Double zeta "MOLOPT" basis sets were used in conjunction with a 1200 Ry cutoff. All cell relaxations were performed without any constraints on the symmetry or the cell parameters. For the four possible configurations of ice IX, we used 2 × 2 × 2 supercells. Direct cell optimizations were performed with a simultaneous update of coordinates and cell parameters.

RESULTS AND DISCUSSION

As shown in Fig. 2(a), the neutron diffraction experiment started with the compression of a 2.5 mol. % ND_4F-doped ice I*h* sample from ambient pressure to 0.3 GPa while increasing the temperature to 210 K. In line with our previous experiments, the compression resulted in the transformation of ice I*h* to ice III and a small amount of the cubic structure II argon clathrate hydrate due to the pressure medium [see Figs. 2(b) and 2(c)].[20] To probe the formation of ice IX, the sample was then cooled to 150 K while keeping the pressure constant at 0.300 GPa. This was achieved over a period of ~12 h while recording powder patterns at least every 10 K.

The formation of ice IX upon cooling can be seen from the merging of the 102 and 201 Bragg peaks around 3 Å as the tetragonal ice III transforms into ice IX, which is close to pseudo-cubic.[9–12] A similar merging of peaks is also seen for the weaker 112 and 211 Bragg peaks just above 2.7 Å. The reversibility of the phase transition is demonstrated upon heating to 220 K when the two groups of peaks split again.

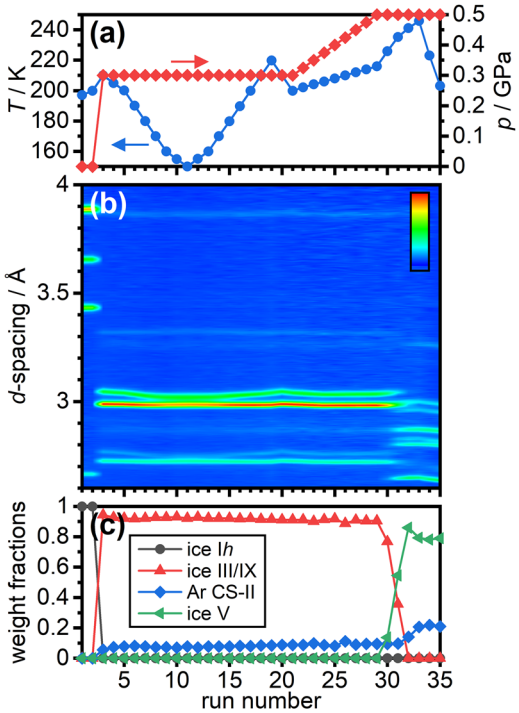

FIG. 2. (a) Changes in temperature and pressure during the neutron diffraction experiment. (b) Neutron diffraction patterns of the D_2O plus 2.5 mol. % ND_4F sample displayed as a contour plot. A color scale bar is shown in the top right-hand corner. (c) Changes in weight fractions of ice I*h*, ice III/IX, cubic structure II argon clathrate hydrate, and ice V as the experiment progressed.

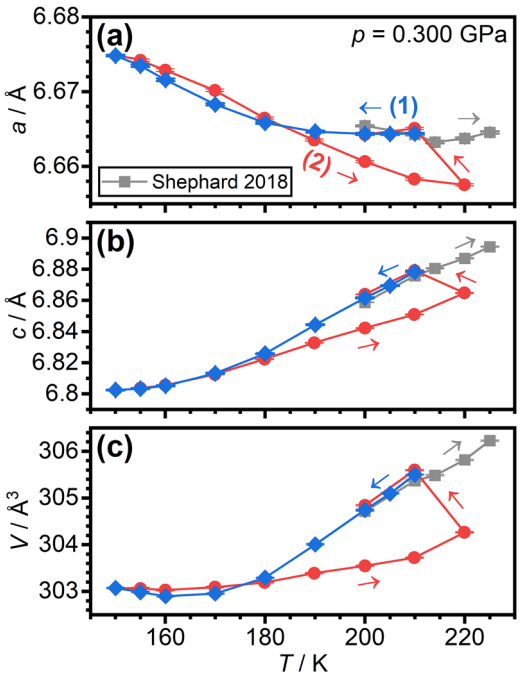

FIG. 3. (a) and (b) Lattice constants and (c) unit-cell volume of D_2O ice III/IX with 2.5 mol. % ND_4F recorded upon cooling from 210 K (blue diamonds) and subsequent heating at 0.3 GPa (red circles). Data points obtained upon heating from 200 K (gray squares) are taken from Ref. 34.

The changes in lattice constants and unit-cell volume upon cooling ice III from 210 K are shown as blue diamonds in Fig. 3. The *a* lattice constant changes very little initially and then begins to increase below 200 K. This change in slope seems to indicate the onset of the phase transition from ice III to ice IX. Interestingly, it is difficult to spot an end point of the phase transition as the *a* lattice constant continues to increase upon cooling below 160 K. In the case of pure ice III, the *a* lattice constant has been shown to contract between 250 K and 240 K at 0.25 GPa.[19] In Ref. 20, we heated a 2.5 mol. % ND_4F sample from 200 K to 250 K. Due to the incongruent melting, only the lattice constants up to 225 K were included as gray squares in Fig. 2. Upon partial melting, the ND_4F may be enriched in the liquid phase, thereby changing the composition of the solid ice phase. This would be problematic since the amount of dissolved ND_4F affects the lattice constants of ice slightly.[20,35,37] For the *a* lattice constant, a minimum is observed in these data at 215 K. All in all, the *a* lattice constant appears to contract at first upon cooling ice III from its region of stability followed by a plateau and then an expansion as the sample undergoes the phase transition to ice IX. This expansion seems to continue upon cooling even once ice IX has fully formed.

The *c* lattice constant contracted as pure ice III is cooled from 250 to 240 K at 0.25 GPa.[19] From the data shown in Fig. 3(b), it can be seen that *c* contracts at all temperatures as our sample was cooled. The most pronounced changes in *c* are observed during the ice III to ice IX phase transition in the 200–170 K temperature range. The temperature range in which the phase transition is observed seems to agree with previous studies of pure ice samples using dielectric spectroscopy,[21] calorimetry,[31] and Raman spectroscopy.[32]

The volume changes of the unit cell in Fig. 3(c) show decreases as ice III is cooled and during the phase transition to ice IX. Interestingly, below 160 K, the volume increases upon cooling to 150 K, which is caused by the expansion in *a*. Anisotropic thermal expansion and overall negative thermal expansion have also been observed for the isostructural keatite[13] and some related *β*-spodumenes ($Li_2O \cdot Al_2O_3 \cdot nSiO_2$).[47] In the case of those materials, the contraction of the *a*–*b* plane upon heating has been explained by the formation of torsional stress as the helical springs expand upon heating. It seems possible that a similar phenomenon is at play in ND_4F-doped ice IX as well at low temperatures and 0.3 GPa. Negative thermal expansion has also been observed for the "ordinary" ice *Ih*.[48,49] However, compared to ice IX, this was observed below 73 K[48] or 60 K,[49] and it did not go along with the anisotropic behavior of the lattice constants. Unfortunately, it was not possible to cool ice IX further at 0.3 GPa because the freezing point of argon would have been reached, which would have resulted in the loss of pressure. In addition, helium or neon could not have been used as the pressure media since they are known to stabilize the ice II structure by intercalation.[50–53]

Heating of the ice IX sample shows some remarkable hysteresis effects. Both the *a* and the *c* lattice constants "overshoot" the phase transition back to ice III upon heating to 220 K, as shown in Fig. 3. In fact, only upon cooling to 210 K from 220 K was equilibrium established, and the lattice constants agreed with those of the ice III measured before the cooling at both 210 K and 200 K. The sluggish hydrogen-disordering kinetics may be a general feature of the ice IX to ice III phase transition. However, some of this effect could be due to the ND_4F doping, which has previously been shown to slowdown the hydrogen ordering kinetics of the ice VII to ice VIII phase transition.[34] Hydrogen-(dis)ordering phase transitions require the collective reorientation of water molecules along traveling defect pathways within the crystal.[25] The incorporation of ND_4^+ and F^- point defects into the hydrogen-bonded network is thought to terminate such defect pathways, which then overall slows down hydrogen (dis)ordering processes.

The effect of ND_4F doping on the extent of hydrogen (dis)order of ice III at 210 K and of ice IX at 150 K was investigated in a next step. Figure 4 shows the Rietveld fits to the diffraction data at these two temperatures. For ice III at 210 K, the two order parameters were refined as $\alpha = 0.456$ and $\beta = 0.454$. For the shorter runs, it was unfortunately not possible to extract such information. Previously, for pure ice III, these values were determined as 0.36 and 0.53, respectively, at 250 K and 0.3 GPa.[19] The extent of partial order observed in ND_4F-doped ice III at 210 K, therefore, seems to be the consequence of the disordering effect of ND_4F doping on the α parameter and partial ordering due to the lower temperature for β. In any case, both order parameters are slightly below $\frac{1}{2}$, which is already the correct trend with respect to the hydrogen ordering toward ice IX at lower temperatures.

The ND_4F-doped ice IX at 150 K displays $\alpha = 0.137$ and $\beta = 0.169$. For pure D_2O ice IX, α and β were determined as 0.034 and 0.051, respectively, highlighting a small degree of residual hydrogen disorder in ice IX.[12] This illustrates that the ND_4F doping is capable of inducing hydrogen disorder within ice IX as it has been previously observed for ice VIII.[34] However, it is important to point

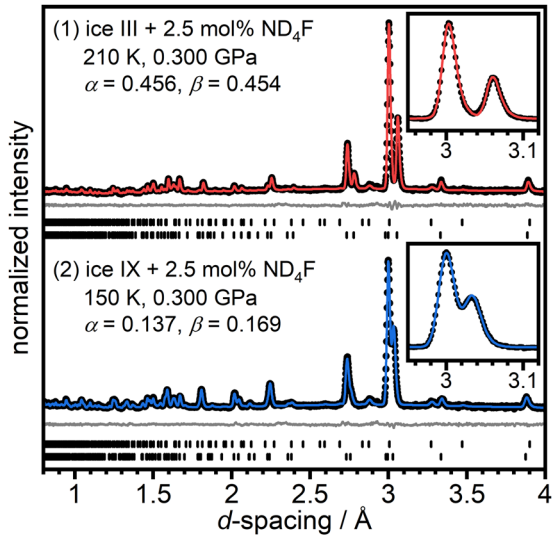

FIG. 4. Rietveld analysis of (1) ND_4F-doped ice III at 210 K and 0.3 GPa and (2) ND_4F-doped ice IX at 150 K and 0.3 GPa. The experimental data are shown as black circles, red or blue lines are the Rietveld fits, and gray lines are the differences between the experimental data and the Rietveld fits downshifted for clarity. The tick marks under each diffraction pattern are for ice III/IX (bottom) and cubic structure II argon clathrate hydrate[54] (top). The two insets show magnifications of the most intense peaks.

out that the way ice IX becomes hydrogen-ordered is not changed by the ND_4F dopant. In principle, either one or both of the order parameters could tend toward one instead of zero and, thereby, form a different hydrogen-ordered structure. In addition, as previously observed for pure ice IX, $\alpha < \beta$ for the ND_4F-doped sample, indicating that the hydrogen sites that are more disordered in pure ice IX are also more disordered in the ND_4F-doped sample. The complete crystallographic information of the ND_4F-doped ice IX is given in Table I.

The incorporation of lithium halides into ice VII has been shown to result in "diffuse Huang scattering."[55,56] This means that the dopant causes a local distortion of the crystalline structure of the parent material, which manifests in "tails" at the Bragg peaks. Close inspection of the shapes of the most intense Bragg peaks of our diffraction data of ND_4F-doped ices III/IX shows an absence of such scattering features (cf. insets in Fig. 4). The absence of diffuse Huang scattering could have two reasons. First, we used a smaller salt to water ratio of 1:40 compared to the 1:6 ratio used by Klotz *et al.*[55,56] Second, as discussed earlier, the hydrogen bond lengths between the NH_4^+ and F^- ions and H_2O are quite similar compared to those in pure ice. The incorporation of those ions into ice is, therefore, expected to lead to quite small local distortions and, hence, no significant Huang scattering. The small effects on the intensities of the Bragg peaks, due to the different scattering lengths of N and F with respect to O, are fully captured in the Rietveld refinements using the model shown in Table I.

The hydrogen-disordering effect of ammonium fluoride doping on ice IX was also followed spectroscopically. Figure 5 shows the decoupled O–D stretching modes of pure and ammonium fluoride doped H_2O ice IX samples containing 5 mol. % deuterium. The spectra were recorded at 80 K and ambient pressure. Decoupled stretching modes of ice arise from spatially separated O–D oscillators within H_2O materials and are, therefore, not affected by the intra- and intermolecular coupling that is seen for the O–H stretching modes.[57,58] The peak position of a decoupled O–D stretching mode has been shown to correlate with the length of the corresponding hydrogen bond.[59,60] The orientational disorder of the water molecules in hydrogen-disordered phases of ice induces positional disorder of the oxygen atoms, which then leads to broader spectroscopic features in the decoupled O–D stretching modes. Hydrogen-ordered phases of ice on the other hand display sharp spectroscopic features in the decoupled O–D stretching mode region.[32,61–65]

The Raman spectrum of pure ice IX shown in Fig. 5 is consistent with other spectra in the literature.[62] The hydrogen order is reflected in two rather sharp spectroscopic features at 2451 cm^{-1} and

TABLE I. Fractional atomic coordinates, fractional occupancies, order parameters and isotropic atomic–displacement parameters (U_{iso}) of D_2O $P4_12_12$ ice IX with 2.5 mol. % ND_4F at 150 K and 0.300 GPa. The lattice constants are a = 6.672 55(8) Å and c = 6.800 55(15) Å. Numbers in parentheses are statistical errors of the last significant digit of refined quantities. The occupancies related to the oxygen, nitrogen and fluorine atoms were calculated from the ND_4F concentration of the initial solution.

Atom label	Atom type	x	y	z	Occupancy	Order parameter	$U_{iso} * 100$
O1	O	0.1022(3)	0.3028(3)	0.2861(4)	0.9512	...	2.90(4)
O2	O	0.3908(4)	0.3908(4)	0.0000	0.9512	...	2.90(4)
D3	D	0.2181	0.3289	0.1809	0.136(1)	α	2.96(2)
D4	D	0.1344	0.3930	0.3866	0.169(1)	β	2.96(2)
D5	D	0.0188(5)	0.3337(3)	0.2145(3)	0.831(1)	$1-\beta$	2.96(2)
D6	D	0.1152(4)	0.1624(3)	0.3035(3)	0.863(1)	$1-\alpha$	2.96(2)
D7	D	0.3009(3)	0.3604(4)	0.1070(3)	0.864(1)	$1-\alpha$	2.96(2)
D8	D	0.3687	0.5494	−0.0216	0.137(1)	α	2.96(2)
N1	N	0.1022(3)	0.3028(3)	0.2861(4)	0.0244	...	2.90(4)
N2	N	0.3908(4)	0.3908(4)	0.0000	0.0244	...	2.90(4)
F1	F	0.1022(3)	0.3028(3)	0.2861(4)	0.0244	...	2.90(4)
F2	F	0.3908(4)	0.3908(4)	0.0000	0.0244	...	2.90(4)

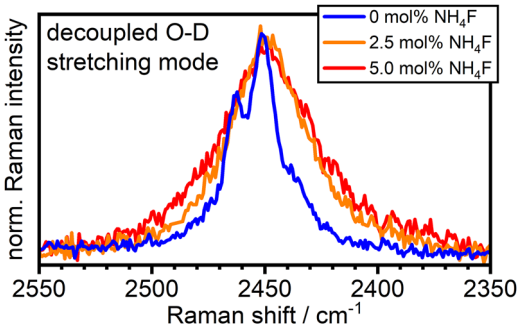

FIG. 5. Raman spectra (λ_0 = 633 nm) of the decoupled O–D stretching modes of pure ice IX and doped with 2.5 mol. % and 5.0 mol. % NH_4F. All samples contain 5 mol. % deuterium. The spectra were collected at 80 K and ambient pressure.

2462 cm^{-1}. The addition of 2.5 mol. % NH_4F leads to significant broadening so that the entire spectroscopic feature appears as one broad peak. The full-width-at-half-height (FWHH) of the feature increases from 40 to 44 cm^{-1} as the amount of NH_4F is increased from 2.5 to 5.0 mol. %. The general shape of the spectroscopic feature resembles that of ice III previously collected at 0.28 GPa and 246 K.[62] In addition to the neutron diffraction data presented earlier, these spectroscopic effects illustrate the hydrogen-disordering effect of NH_4F doping very nicely. In line with the changes in lattice constants and computational calculations in Ref. 20, the spectra also indicate that the NH_4F dopant forms a solid solution with the ice IX. Any phase separation between NH_4F and H_2O would be expected to result in the formation of a small sharp feature associated with the decoupled NH_3–D mode of pure ammonium fluoride.

With the report of the hydrogen-disordering effect of NH_4F doping on ice IX, it has now been established that all phases of ice that hydrogen-order without the help of a dopant upon cooling can be hydrogen-disordered with NH_4F. In a next step, it is interesting to compare the extent of the hydrogen-disordering effect of NH_4F on these phases. In the case of fully hydrogen-ordered ice VIII, doping with 2.5 mol. % NH_4F changed the single order parameter from 0 to 0.156.[34] As mentioned above, for ice IX, the changes using the same amount of NH_4F doping are 0.034 → 0.137 and 0.051 → 0.169, which correspond to changes of 0.103 and 0.118, respectively. The hydrogen-disordering effect of 2.5 mol. % NH_4F is, therefore, slightly less in ice IX than it was for the fully hydrogen-ordered ice VIII. For the fully hydrogen-ordered ice II, the disordering effect of NH_4F was to such an extent that it led to its complete destabilization.[20]

The presence of residual hydrogen disorder in pure ice IX as opposed to the pure ices II and VIII implies a higher density of partially disordered states close to the energetic ground state. This is now nicely illustrated by the NH_4F doping experiments. In a sense, NH_4F doping can be seen as a chemical way to achieve "excitation" within the configurational ice-rules manifold. Compared to the partially disordered ice IX, the NH_4F doping achieves a greater "excitation" away from the ground state in the cases of the fully hydrogen-ordered ices II and VIII.

Since the changes in lattice constants determined earlier were obtained from a ND_4F-doped sample, it is interesting in a next step to ask the question if the changes would be similar for pure ice III/IX samples. To address this question, lattice constants for the four possible hydrogen-ordered arrangements of ice IX in $P4_12_12$ were calculated using Density Functional Theory (DFT) both with and without considering dispersion interactions[46] using the PBE functional.[66,67] The results are shown in Fig. 6 as the ratios of the lattice constants with respect to the averages of all four configurations. This is thought to provide a measure for how the lattice constants behave relative to the hydrogen-disordered state.

The first configuration, with $\alpha = 0$ and $\beta = 0$, corresponds to the experimental configuration found for ice IX both previously and in this study. The DFT calculations predict a small increase in a and a more substantial decrease in c for the transition from ice III to ice IX. Including dispersion interactions in the calculations makes both changes somewhat larger. For the second configuration ($\alpha = 1$ and $\beta = 0$), the same trends are observed. However, the changes in the lattice constants are more pronounced. Reverse trends with a contracting and c expanding are predicted for the third configuration ($\alpha = 0$ and $\beta = 1$), which is in clear contradiction with the experimental observations. Finally, the fourth configuration ($\alpha = 1$ and $\beta = 1$) displays weakly positive changes for both lattice constants. From the changes in lattice constants determined in Fig. 3, it is difficult to extract accurate values for the hydrogen ordering phase transition since the temperature window of the phase transition is large and the effects of temperature overlap with those from the ordering transition. Nevertheless, the predicted changes for configurations 3 and 4 are in clear disagreement with the experimental observations. The changes predicted by the second configurations are significantly too large considering the experimental changes. For example, if a c value of 6.8 Å is taken for ice IX, this would imply a c lattice constant for ice III of about 7.08 Å, which is clearly outside the experimentally feasible range. The predicted changes in the lattice constants of the first configuration are the ones that most closely resemble the experimental ones of the doped sample. Including dispersion interactions appears to be important for achieving c/a ratios close to the pseudo-cubic experimental structure of ice IX. The ratios changed from 1.13 to 1.05 upon including dispersion interactions for the first configuration.

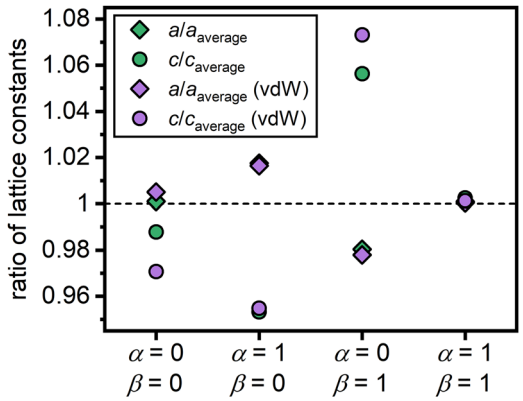

FIG. 6. Ratios of the calculated lattice constants of the four possible ice IX configurations with order parameters α and β divided by the averages of all four configurations. The ratios are given with and without considering dispersion interactions in the calculations.

It is interesting to note that the volume change for the ice III to ice IX phase transition is negative. This is in contrast with the ice VI to ice XV phase transition for which a positive volume change has been observed upon hydrogen ordering.[68] The positive volume change enabled us to suppress hydrogen ordering at pressures leading up to ~1 GPa and to isolate so-called "deep glassy states" of ice VI.[69,70] Considering the negative volume change of the ice III to ice IX phase transition, obtaining hydrogen-disordered ice III at low temperatures by increasing the pressure seems, therefore, difficult. However, a way forward could be to increase the ammonium fluoride concentration beyond 2.5 mol. %, which is expected to further slowdown the hydrogen kinetics upon cooling. Interesting trends in the lattice constants have also recently been observed for the ice VII to ice VIII phase transition.[71] However, it is at present unclear if the volume change is positive or negative.

In a final step of the neutron diffraction experiment, the ice III sample was compressed to 0.5 GPa while heating from 200 to 246 K, as shown in Figs. 1(a) and 2. Consistent with our previous piston–cylinder experiments,[20] the phase transition to ice V was observed at about 0.4 GPa. Upon cooling from 246 to 203 K, which is within the region of stability of ice II in the case of pure ice, the ice V persisted as expected since the ND_4F doping prevents the formation of ice II.

To explore the disappearance of ice II at 0.5 GPa upon the addition of NH_4F more systematically, pure and NH_4F-doped H_2O ice I*h* samples were heated isobarically at 0.5 GPa while recording the volume changes. The resulting data are shown in Fig. 7 as a three-dimensional contour plot in analogy with the corresponding figure for 0.3 GPa in Ref. 20. Following a metastable "plateau" of ice III/IX between about 170 and 190 K, ice II disappears between 0.1 and 0.25 mol. % NH_4F and is entirely replaced by the *denser* ice V from 0.25 mol. % onward. This is in contrast to the situation at 0.3 GPa, where the *less dense* ice III exists instead of ice II.[20] Furthermore, at

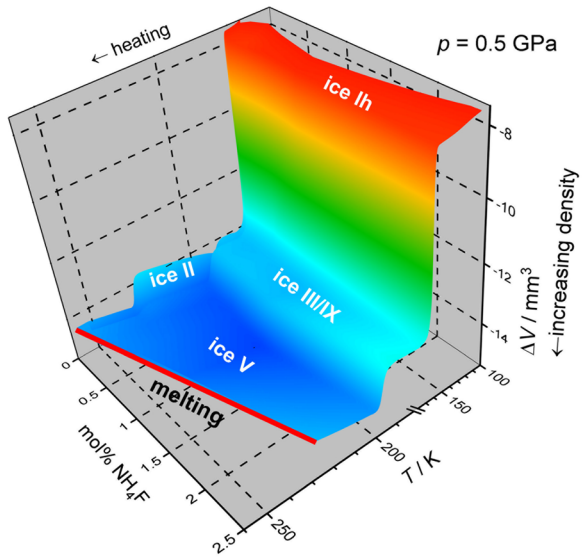

FIG. 7. Volume changes recorded upon isobaric heating at 0.5 GPa of pure ice I*h* and doped samples with 0.05, 0.10, 0.25, 0.50, 1.00, and 2.50 mol. % NH_4F.

0.3 GPa, slightly larger amounts of NH_4F between 0.25 and 0.50 mol. % were required for the complete disappearance of ice II. In Ref. 20, we argued that the ice II disappearance starts when the solubility limit of NH_4F in the coexisting hydrogen-disordered phase is reached. The slightly smaller amounts of NH_4F required at 0.5 GPa compared to 0.3 GPa, therefore, suggest that NH_4F is less soluble in ice V than it is in ice III.

CONCLUSIONS

The ice III to ice IX phase transition of samples doped with 2.5 mol. % ND_4F was followed with *in situ* neutron diffraction. The hydrogen ordering phase transition in the 200 to 170 K temperature window goes along with an expansion in the *a* lattice constant and contraction in *c*, which corresponds to the shrinking of the helical springs in the crystal structure. Overall, the volume decreases during the ice III to ice IX phase transition. Below 160 K, the *a* lattice constant continues to expand, which interestingly leads to a volume expansion as the ice IX is cooled. This unusual behavior has previously been observed for the isostructural keatite and related spodumene materials and has been attributed to the buildup of torsional strain within the *a*–*b* plane as the helical "springs" contract.

The reversibility of the ice IX to ice III phase transition upon heating has been demonstrated including significant hysteresis effects. This may be enhanced by the ND_4F dopant, which is known to slowdown hydrogen (dis)ordering kinetics. Interestingly, the hydrogen-disordering effect of ND_4F on ice IX was found to be less compared to ice VIII. This led us to propose that doping with ammonium fluoride can be regarded as a chemical way to achieve "excitation" of the configurational ice-rules manifold. In the case of ice IX, the ND_4F doping indicates a higher density of states close to the ordered ground state compared to, for example, ices II and VIII. It can now also be concluded that all hydrogen-ordered phases of ice that form in the absence of dopants (i.e., ices IX and VIII) can be hydrogen-disordered with ammonium fluoride doping. These findings underpin once more the highly complex solid-state chemistry of ice.

ACKNOWLEDGMENTS

We acknowledge the European Research Council under the European Union's Horizon 2020 research and innovation program (Grant Agreement No. 725271) for funding and the Advanced Characterization of Materials CDT for a studentship (Grant No. EP/L015277/1). We thank ISIS for granting access to the PEARL instrument, and we are grateful to C. Ridley (ISIS crystallography group), C. Goodway, and M. Kibble (ISIS pressure support) for help with the neutron diffraction experiment. We acknowledge the use of ARCHER via our membership of the UK's HEC Materials Chemistry Consortium, which is funded by EPSRC (Grant Nos. EP/L000202 and EP/R029431).

DATA AVAILABILITY

Raw data were generated at the ISIS large scale facility. Derived data supporting the findings of this study are available from the corresponding author upon reasonable request. The raw data are available at https://doi.org/10.5286/ISIS.E.86391366.

REFERENCES

[1] C. G. Salzmann, J. Chem. Phys. **150**, 060901 (2019).
[2] M. Millot, F. Coppari, J. R. Rygg, A. Correa Barrios, S. Hamel, D. C. Swift, and J. H. Eggert, Nature **569**, 251 (2019).
[3] G. Tammann, Ann. Phys. **2**, 1 (1900).
[4] P. W. Bridgman, J. Chem. Phys. **5**, 964 (1937).
[5] P. W. Bridgman, Proc. Am. Acad. Arts Sci. **47**, 441 (1912).
[6] K. Echelmeyer and B. Kamb, Geophys. Res. Lett. **13**, 693, https://doi.org/10.1029/gl013i007p00693 (1986).
[7] F. Sohl, T. Spohn, D. Breuer, and K. Nagel, Icarus **157**, 104 (2002).
[8] W. B. Durham, S. H. Kirby, and L. A. Stern, J. Geophys. Res. **102**, 16293, https://doi.org/10.1029/97je00916 (1997).
[9] W. B. Kamb and S. K. Datta, Nature **187**, 140 (1960).
[10] B. Kamb and A. Prakash, Acta Crystallogr., Sect. B: Struct. Crystallogr. Cryst. Chem. **24**, 1317 (1968).
[11] S. W. Rabideau, E. D. Finch, G. P. Arnold, and A. L. Bowman, J. Chem. Phys. **49**, 2514–2519 (1968).
[12] S. J. La Placa and W. C. Hamilton, J. Chem. Phys. **58**, 567 (1973).
[13] P. P. Keat, Science **120**, 328 (1954).
[14] L. del Rosso, F. Grazzi, M. Celli, D. Colognesi, V. Garcia-Sakai, and L. Ulivi, J. Phys. Chem. C **120**, 26955 (2016).
[15] G. J. Wilson, R. K. Chan, D. W. Davidson, and E. Whalley, J. Chem. Phys. **43**, 2384 (1965).
[16] E. Whalley and D. W. Davidson, J. Chem. Phys. **43**, 2148 (1965).
[17] J. D. Londono, W. F. Kuhs, and J. L. Finney, J. Chem. Phys. **98**, 4878 (1993).
[18] W. F. Kuhs, C. Lobban, and J. L. Finney, Rev. High Pressure Sci. Technol. **7**, 1141 (1998).
[19] C. Lobban, J. L. Finney, and W. F. Kuhs, J. Chem. Phys. **112**, 7169 (2000).
[20] J. J. Shephard, B. Slater, P. Harvey, M. Hart, C. L. Bull, S. T. Bramwell, and C. G. Salzmann, Nat. Phys. **14**, 569 (2018).
[21] E. Whalley, J. B. R. Heath, and D. W. Davidson, J. Chem. Phys. **48**, 2362 (1968).
[22] K. Vonnegut, *Cat's Cradle* (Holt, Rinehart and Winston, New York, 1963).
[23] V. F. Petrenko and R. W. Whitworth, *Physics of Ice* (Oxford University Press, Oxford, 1999).
[24] C. G. Salzmann, E. Mayer, and A. Hallbrucker, Phys. Chem. Chem. Phys. **6**, 5156 (2004).
[25] C. G. Salzmann, P. G. Radaelli, J. L. Finney, and E. Mayer, Phys. Chem. Chem. Phys. **10**, 6313 (2008).
[26] A. J. Leadbetter, R. C. Ward, J. W. Clark, P. A. Tucker, T. Matsuo, and H. Suga, J. Chem. Phys. **82**, 424 (1985).
[27] J. D. Jorgensen, R. A. Beyerlein, N. Watanabe, and T. G. Worlton, J. Chem. Phys. **81**, 3211 (1984).
[28] C. G. Salzmann, P. G. Radaelli, A. Hallbrucker, E. Mayer, and J. L. Finney, Science **311**, 1758 (2006).
[29] C. G. Salzmann, P. G. Radaelli, E. Mayer, and J. L. Finney, Phys. Rev. Lett. **103**, 105701 (2009).
[30] C. Knight and S. J. Singer, J. Chem. Phys. **125**, 064506 (2006).
[31] K. Nishibata and E. Whalley, J. Chem. Phys. **60**, 3189 (1974).
[32] B. Minceva-Sukarova, W. F. Sherman, and G. R. Wilkinson, J. Mol. Struct. **115**, 137 (1984).
[33] G. P. Arnold, R. G. Wenzel, S. W. Rabideau, N. G. Nereson, and A. L. Bowman, J. Chem. Phys. **55**, 589 (1971).
[34] C. G. Salzmann, Z. Sharif, C. L. Bull, S. T. Bramwell, A. Rosu-Finsen, and N. P. Funnell, J. Phys. Chem. C **123**, 16486 (2019).
[35] R. Brill and S. Zaromb, Nature **173**, 316 (1954).
[36] L. C. Labowitz and E. F. Westrum, J. Phys. Chem. **65**, 403 (1961).
[37] L. C. Labowitz and E. F. Westrum, J. Phys. Chem. **65**, 408 (1961).
[38] J. J. Shephard, S. Ling, G. C. Sosso, A. Michaelides, B. Slater, and C. G. Salzmann, J. Phys. Chem. Lett. **8**, 1645 (2017).
[39] A. K. Lyashchenko and G. G. Malenkov, Zh. Strukt. Khim. **10**, 724 (1969).
[40] K. Shin, I. L. Moudrakovski, M. D. Davari, S. Alavi, C. I. Ratcliffe, and J. A. Ripmeester, CrystEngComm **16**, 7209 (2014).
[41] S. Park, D. Lim, Y. Seo, and H. Lee, Chem. Commun. **51**, 8761 (2015).
[42] C. L. Bull, N. P. Funnell, M. G. Tucker, S. Hull, D. J. Francis, and W. G. Marshall, High Pressure Res. **36**, 493 (2016).
[43] A. C. Larsen and R. B. Von Dreele, *GSAS–General Structure Analysis System* (University of California, 1985).
[44] Z. Sharif, Ph.D. thesis, University College London, London, 2020.
[45] T. D. Kühne, M. Iannuzzi, M. Del Ben, V. V. Rybkin, P. Seewald, F. Stein, T. Laino, R. Z. Khaliullin, O. Schütt, F. Schiffmann, D. Golze, J. Wilhelm, S. Chulkov, M. H. Bani-Hashemian, V. Weber, U. Borštnik, M. Taillefumier, A. S. Jakobovits, A. Lazzaro, H. Pabst, T. Müller, R. Schade, M. Guidon, S. Andermatt, N. Holmberg, G. K. Schenter, A. Hehn, A. Bussy, F. Belleflamme, G. Tabacchi, A. Glöß, M. Lass, I. Bethune, C. J. Mundy, C. Plessl, M. Watkins, J. VandeVondele, M. Krack, and J. Hutter, J. Chem. Phys. **152**, 194103 (2020).
[46] S. Grimme, J. Antony, S. Ehrlich, and H. Krieg, J. Chem. Phys. **132**, 154104 (2010).
[47] W. Ostertag, G. R. Fischer, and J. P. Williams, J. Am. Ceram. Soc. **51**, 651 (1968).
[48] K. Röttger, A. Endriss, J. Ihringer, S. Doyle, and W. F. Kuhs, Acta Crystallogr., Sect. B: Struct. Sci. **50**, 644 (1994).
[49] A. D. Fortes, Acta Crystallogr., Sect. B: Struct. Sci., Cryst. Eng. Mater. **74**, 196 (2018).
[50] C. Lobban, J. L. Finney, and W. F. Kuhs, J. Chem. Phys. **117**, 3928 (2002).
[51] D. Londono, J. L. Finney, and W. F. Kuhs, J. Chem. Phys. **97**, 547 (1992).
[52] D. Londono, W. F. Kuhs, and J. L. Finney, Nature **332**, 141 (1988).
[53] X. Yu, J. Zhu, S. Du, H. Xu, S. C. Vogel, J. Han, T. C. Germann, J. Zhang, C. Jin, J. S. Francisco, and Y. Zhao, Proc. Natl. Acad. Sci. U. S. A. **111**, 10456 (2014).
[54] A. Y. Manakov, V. I. Voronin, A. V. Kurnosov, A. E. Teplykh, V. Y. Komarov, and Y. A. Dyadin, J. Inclusion Phenom. **48**, 11 (2004).
[55] S. Klotz, L. E. Bove, T. Strässle, T. C. Hansen, and A. M. Saitta, Nat. Mater. **8**, 405 (2009).
[56] S. Klotz, K. Komatsu, F. Pietrucci, H. Kagi, A. A. Ludl, S. Machida, T. Hattori, A. Sano-Furukawa, and L. E. Bove, Sci. Rep. **6**, 32040 (2016).
[57] C. Haas and D. F. Hornig, J. Chem. Phys. **32**, 1763 (1960).
[58] D. Eisenberg and W. Kauzmann, *The Structure and Properties of Water* (Plenum Press, Oxford, 1969), Vol. 1.
[59] W. F. Kuhs and M. S. Lehmann, in *Science Reviews*, edited by F. Franks (Cambridge University Press, Cambridge, UK, 1986), Vol. 2, p. 1.
[60] C. A. Tulk, D. D. Klug, R. Branderhorst, P. Sharpe, and J. A. Ripmeester, J. Chem. Phys. **109**, 8478 (1998).
[61] B. Minceva-Sukarova, W. F. Sherman, and G. R. Wilkinson, Spectrochim. Acta, Part A **41**, 315 (1985).
[62] B. Minceva-Sukarova, W. F. Sherman, and G. R. Wilkinson, J. Phys. C: Solid State Phys. **17**, 5833 (1984).
[63] T. F. Whale, S. J. Clark, J. L. Finney, and C. G. Salzmann, J. Raman Spectrosc. **44**, 290 (2013).
[64] C. G. Salzmann, A. Hallbrucker, J. L. Finney, and E. Mayer, Chem. Phys. Lett. **429**, 469 (2006).
[65] C. G. Salzmann, A. Hallbrucker, J. L. Finney, and E. Mayer, Phys. Chem. Chem. Phys. **8**, 3088 (2006).
[66] J. P. Perdew, K. Burke, and M. Ernzerhof, Phys. Rev. Lett. **77**, 3865 (1996).
[67] J. P. Perdew, K. Burke, and M. Ernzerhof, Phys. Rev. Lett. **78**, 1396 (1997).
[68] C. G. Salzmann, B. Slater, P. G. Radaelli, J. L. Finney, J. J. Shephard, M. Rosillo-Lopez, and J. Hindley, J. Chem. Phys. **145**, 204501 (2016).
[69] A. Rosu-Finsen and C. G. Salzmann, Chem. Sci. **10**, 515 (2019).
[70] A. Rosu-Finsen, A. Amon, J. Armstrong, F. Fernandez-Alonso, and C. G. Salzmann, J. Phys. Chem. Lett. **11**, 1106 (2020).
[71] K. Komatsu, S. Klotz, S. Machida, A. Sano-Furukawa, T. Hattori, and H. Kagi, Proc. Natl. Acad. Sci. U. S. A. **117**, 6356 (2020).